remote sensing

MDPI

Article

Research on Multi-Domain Dimensionality Reduction Joint Adaptive Processing Method for Range Ambiguous Clutter of FDA-Phase-MIMO Space-Based Early Warning Radar

Tianfu Zhang [1], Zhihao Wang [1], Mengdao Xing [1], Shuangxi Zhang [2] and Yongliang Wang [1,3,*]

[1] The National Laboratory of Radar Signal Processing, Xidian University, Xi'an 710071, China
[2] School of Electronics and Information, Northwestern Polytechnical University, Xi'an 710072, China
[3] Key Research Laboratory, Wuhan Radar Academy, Wuhan 430019, China
* Correspondence: ylwangkjld@163.com

Abstract: The ground and sea clutter received by space-based early warning radar (SBEWR) has severely range ambiguous characteristics due to its platform location, and the non-stationary factor caused by Earth's rotation makes the received clutter at different range ambiguous positions seriously broaden in the Doppler dimension. The complex clutter suppression performance of SBEWR obtained by traditional method is degraded significantly. To solve this problem and achieve better clutter suppression performance, a novel multi-domain adaptive processing method for clutter suppression is proposed in this paper. The proposed method introduced a range related signal processing domain based on conventional space–time domain by using frequency diverse array phase multiple-input multiple-output (FDA-Phase-MIMO) radar. In addition, a novel multi-domain joint dimensionality reduction structure was designed. The novel multi-domain joint adaptive processing using the proposed dimensionality reduction structure could not only obtain great clutter suppression performance of SBEWR, but also minimize the requirement of the number of selected auxiliary channels. Simulation examples show the effectiveness of the proposed method.

Keywords: space-based early warning radar (SBEWR); space–time adaptive processing (STAP); frequency diverse array (FDA); range-ambiguous clutter suppression; multi-domain signal processing

Citation: Zhang, T.; Wang, Z.; Xing, M.; Zhang, S.; Wang, Y. Research on Multi-Domain Dimensionality Reduction Joint Adaptive Processing Method for Range Ambiguous Clutter of FDA-Phase-MIMO Space-Based Early Warning Radar. *Remote Sens.* **2022**, *14*, 5536. https://doi.org/10.3390/rs14215536

Academic Editors: Jingwei Xu, Keqing Duan, Weijian Liu and Xiongpeng He

Received: 30 August 2022
Accepted: 28 October 2022
Published: 2 November 2022

1. Introduction

The space-based early warning radar (SBEWR) in low earth orbit (LEO) can obtain a greater maximum detectable distance, wider early warning surveillance region, and much longer warning time [1–3]. Especially for hypersonic targets in near space that have a small radar cross section (RCS), the early warning radar systems on satellite platforms perform advantages that are inimitable by traditional airborne early warning radars (AEWRs). In general, the moving targets are detected in the power spectrum of the received signal, but the faint targets are usually submerged in the clutter and system noise [4]. Therefore, clutter suppression plays an important role in moving target detection [5–8]. Moreover, the SBEWR in LEO gains the above early warning advantages due to its platform height but also makes the received clutter more complex in actuality, which brings a series of serious challenges to the clutter suppression assignment [9,10].

Compared with the AEWRs, the clutter received by SBEWR is more difficult to suppress, mainly due to the different platforms on which they are located. The SBEWR platform has extremely high height and fast velocity; these two factors together lead the received clutter to have serious range ambiguity and Doppler ambiguity [11,12]. In addition, an additional Doppler shift into the received ground–sea clutter is introduced by Earth's rotation. This non-stationary factor, which causes the Doppler frequencies of different clutter receiving patches with the same incidence cone angle to no longer coincide, leads to a severe broadening of the received clutter Doppler spectrum, which in severe cases

even occupies the entire Doppler frequency band [13]. Spectral spreading leads to a serious increase in the degrees of freedom (DOFs) of received clutter, making the conventional two-dimensional (2D) space–time adaptive processing (STAP) system insufficient in its degrees of freedom and the performance of clutter suppression and moving target detection severely degraded [14–17]. Therefore, to detect faint moving targets with small radar cross sections (RCS) and implement the AMTI function, it is necessary to improve this phenomenon of range ambiguous clutter heavily spreading in the Doppler dimension.

Some scholars have recently proposed many methods to improve the range ambiguity clutter suppression performance. These former clutter suppression methods can be divided into two main types: firstly, the severely range ambiguous clutter is suppressed by means of pre-processing, after which the DOFs of received clutter meet the requirement of being less than the DOFs of the adaptive system, and the adaptive clutter suppression capability is thus improved. For example, the signal processing domains related to the range dimension, such as the antenna elevation dimension received channel domain, the transmit pulse phase encoding domain, and transmit carrier frequency domain, are introduced in [18–21], respectively. The method proposed in [18–21] used different 3D cascaded processing methods to suppress the range ambiguous clutter. These cascaded processing methods firstly preprocess the received data by the newly introduced dimension and then suppress the preprocessed clutter using the traditional 2D STAP method. Secondly, by increasing the DOFs of the adaptive system, the system also could achieve better adaptive processing performance. KeQing Duan et al. [22,23] proposed an adaptive processing method for 3D joint dimensionality reduction. Instead of using cascaded signal processing, this approach proposed multiple 3D joint dimensionality reduction structures, the proposed method could obtain good non-stationary clutter suppression with sufficient DOFs and the required number of training samples by designing a reasonable dimensionality reduction structure. Actually, most of these past multi-domain processing methods are proposed for non-side-looking AEWRs, while the SBEWR receives clutter with extremely high DOFs in the elevation dimension, and the antenna elevation dimension is often very limited. The ideal clutter suppression performance cannot be obtained by introducing 3D cascade or joint methods in the elevation dimension channel domain.

The key to the clutter suppression method is the adequacy of the obtained clutter information. On the basis of digital antenna technology, the frequency diverse array phase multiple-input multiple-output (FDA-Phase-MIMO) radar is widely applied [24–26]; this radar could use signal processing methods to obtain 3D clutter data in the transmitting carrier frequency domain-receive array element (subarray) domain-pulse domain. In this paper, a novel 3D joint dimensionality reduction adaptive processing method for clutter suppression based on FDA-Phase-MIMO radar is proposed, the design method of the 3D joint dimensionality reduction structure has also been analyzed in detail, and a better dimensionality reduction structure is designed. The proposed method can not only obtain great performance of severely range ambiguous clutter suppression and achieve the desired performance of moving target detection, but also the number of training samples required for accurate estimation of the clutter covariance matrix is about half of that of the traditional 3D joint domain localized (JDL) structure. In addition, the DOFs of the transmit carrier frequency domain are no longer limited by the number of channels in the elevation dimension of the antenna, which theoretically allows the system to obtain higher DOFs for signal processing in the range dimension.

The rest of this paper is outlined as follows. The geometric model, antenna divided model, and the FDA-Phase-MIMO signal model of SBEWR are established in Section 2. In Section 3, multi-domain radar signal processing methods are elucidated in detail, and different multi-domain joint dimensionality reduction structures are proposed. Section 4 illustrates the experimental results and analysis of the performance. Finally, Section 5 concludes the article.

2. SBEWR Working Model and Problem Formulation

2.1. Geometric Model of SBEWR

A geometric model of SBEWR located in LEO is shown in Figure 1. Where, S is the SBEWR moving along the velocity V, which is parallel to the ground, H is the orbital altitude of satellite, O is the center of the earth, R_e is the radius of the earth, B represents the sub-satellite point, θ_{el} and θ_{az} represent the azimuth and elevation angles of the beam, respectively. The beam cone angle is defined as $\cos\psi = \sin\theta_{el}\cos\theta_{az}$.$R_s$ represents the slant distance of the current clutter range cell, and R_{smax} is the maximum detectable distance of the surface that can be covered by the beam of SBEWR, limited by the curvature of the earth.

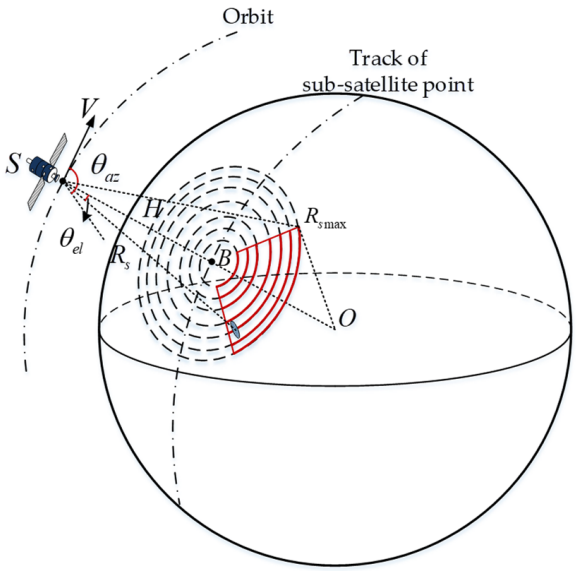

Figure 1. Working geometric model of SBEWR.

Due to the extremely wide region covered by the beam, echoes from different transmitted pulses are superimposed and received simultaneously, which creates severe range ambiguity. The maximum unambiguous distance can be expressed as:

$$r_u = \frac{c}{2f_r} \tag{1}$$

The number of the forward and backward range ambiguous positions of the CUT with slant distance R_s are expressed as:

$$L_{forward} = \left\lfloor \frac{R_{\mathrm{smax}} - R_s}{r_u} \right\rfloor \tag{2}$$

$$L_{backward} = \left\lfloor \frac{R_s - H}{r_u} \right\rfloor \tag{3}$$

The number of total range ambiguous positions N_r is $\left\lfloor \frac{R_{\mathrm{smax}}-H}{r_u} \right\rfloor$; when the orbital altitude is 500 km and the selected pulse repetition frequency (PRF) is 5000 Hz, the total range ambiguity number is about 66. The corresponding slant distance of the nr-th range ambiguous position is

$$R_{nr} = R_s + nr \cdot r_u \ , \ nr \in \left[-L_{backward} : 1 : L_{forward} \right] \tag{4}$$

The elevation angle of each range ambiguous position is:

$$\theta_{el,nr} = \arccos\left(\frac{H^2 + 2R_eH + R_{nr}^2}{2(H + R_e)R_{nr}}\right) \tag{5}$$

According to (5), it can be found that the near-range ambiguous positions corresponding to the elevation angle are discrete distribution, while the far-range ambiguous positions corresponding to the elevation angle are densely distributed. As shown in the red region in Figure 1, according to the J. Ward clutter receiving model [27], the surveillance region is divided into L range cells by range resolution, and to ensure that clutter information is accurate in the simulation, each range cell is divided into N_c azimuth clutter receiving patches, at least according to the Brennan criterion. The theoretical DOFs of sense clutter within the CUT can be expressed as:

$$N_c = DOF_{CUT} = (K-1)\beta_1 + N \tag{6}$$

where

$$\beta_1 = \frac{V_r T_r}{\lambda/2}\sin\theta_{el} = \beta\sin\theta_{el} \tag{7}$$

refers to the Doppler foldover factor. Due to the inconsistent Doppler characteristics of each clutter receiving patch with equal cone angle in different range ambiguous positions, their corresponding clutter subspaces are inconsistent, which leads to a great expansion of the DOFs of the received clutter. According to (5), it can be known that the dense distribution of forward range ambiguous positions makes its subspace distinction obscure. Finally, the total number of DOFs of the true clutter $DOF_{theoretical}$ satisfies (8). The CCM of SBEWR is always nonsingular, and the criterion that the DOFs of the system are larger than the DOFs needed to process clutter cannot be satisfied in the signal processing stage, which will result in insufficient clutter suppression and reduced detection of moving targets.

$$NK < N_c = DOF_{theoretical} < \left\lfloor \frac{R_{\max} - R_{\min}}{r_u} \right\rfloor \times DOF_{CUT} \tag{8}$$

To avoid the lack of DOFs of the system, the adaptive processing performance of the system can be improved either by introducing new processing dimensions to enhance the DOFs of the system or by pre-processing the signal to reduce the DOFs of real clutter. For this purpose, the FDA-Phase-MIMO radar is used to enhance the adaptive capability by introducing the transmitting carrier frequency domain in this paper.

2.2. Antenna Subarray Partition Model

The detailed schematic diagram of FDA-Phase-MIMO radar array element synthesis and transceiver channel division is shown as Figure 2a. Figure 2b shows the transmitted subarray model with array element frequency division multiplexing and transmitting waveform ϕ_m by the m-th channel; unlike the conventional MIMO radar, each transmitted waveform of Phase-MIMO radar can be coherently accumulated with energy at the transmitter in the manner of phased array radar, and the transmitted beam is directional. As shown in Figure 2c, for signal reception, similarly, the received data of the m-th to the $m + N - M_a$-th array element are synthesized, where the local spatial steering vector and Chebyshev weights are generally used as a fixed weighting method for the array element level data; the result of the data accumulation is used as the subarray level data of the m-th received channel for subsequent processing. Figure 2d shows the received subarray synthesis model; the subarray level data output from each receiver channel is output as the output power of the antenna system after weighted synthesis. The weights used for the synthesis between subarrays can be conventional weight, adaptive weights, or a combination of multiple weighting methods.

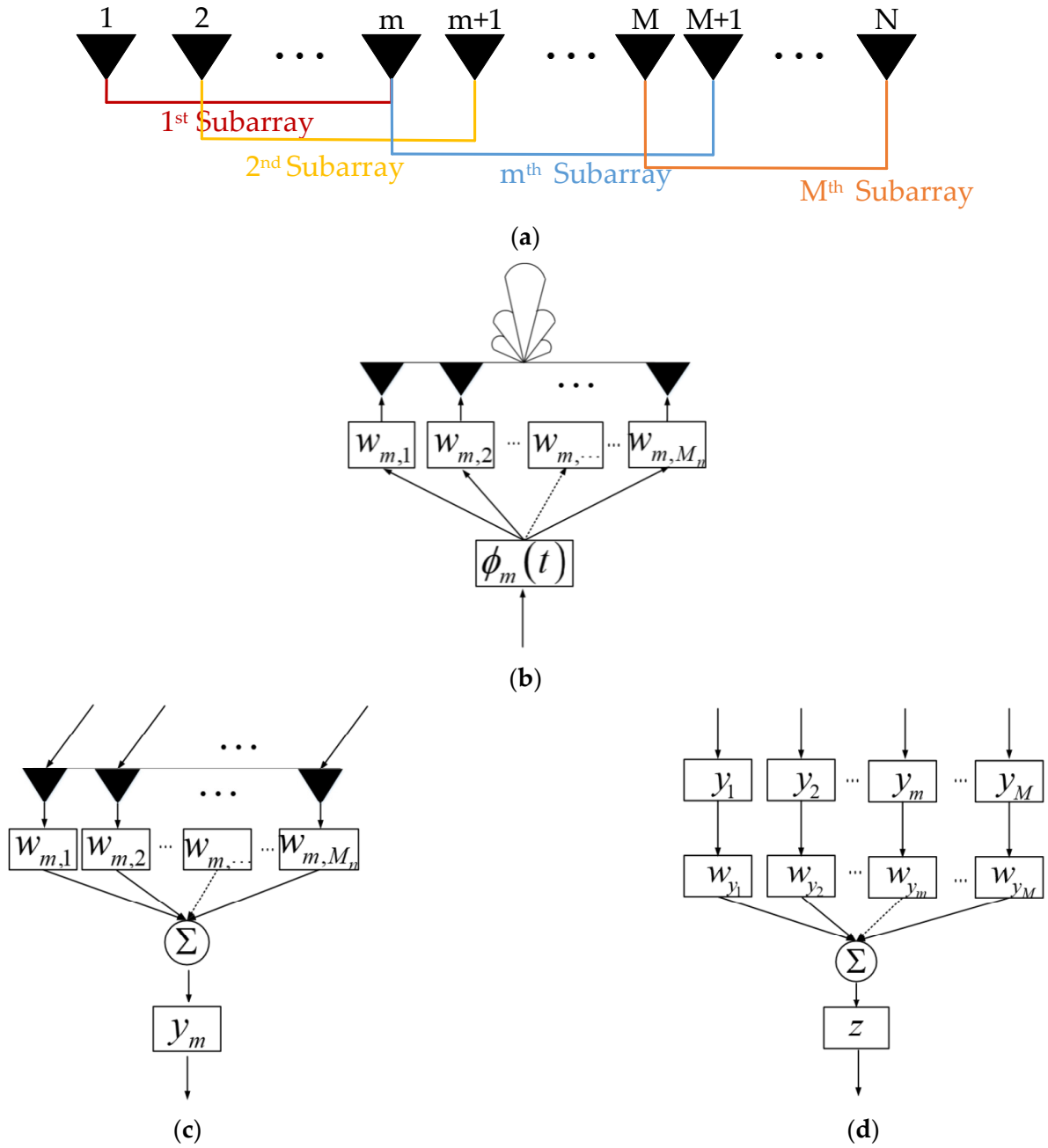

Figure 2. Transceiver channel division model of FDA-Phase-MIMO radar: (**a**) Antenna subarray division model; (**b**) Transmitting subarray model; (**c**) Receiving subarray model; (**d**) Receiving sub-array synthesis model.

2.3. Signal Model

The transmit signal of the m-th subarray of the antenna is:

$$\phi_m(t) = Q_m(t)\exp(j2\pi f_m t) \tag{9}$$

where $Q_m(t)$ represents the amplitude of the transmitted signal and the central frequency is f_m. The frequency of the signals transmitted by the different subarrays is stepped, and the frequency interval is Δf. According to the concept of MIMO radar, the waveforms transmitted by different subarrays are orthogonal to each other, and the transmit waveform vector is expressed as:

$$\mathbf{\Phi}(t) = \begin{bmatrix}\phi_1(t) & \cdots & \phi_M(t)\end{bmatrix}^T \tag{10}$$

The echo received by the radar receiving antenna from a particular target or a clutter received patch is a superposition of m transmitted waveforms, where the echo signal of the k-th pulse received by the n-th array element can be expressed as:

$$\begin{aligned}\bar{r}(t,\psi) = \sum_{m=1}^{M} & A_m \mathbf{w}_m^H \mathbf{a}_m(\psi) \exp\left(-j\tfrac{2\pi}{\lambda} d_{T_m} \cos\psi\right) Q_m(t - t_{dealy}) \exp(j2\pi f_m(t - t_{delay})) \\ & \times \exp(-j\pi \cos\psi(n-1)) \exp(-j\pi\omega_d(k-1))\end{aligned} \tag{11}$$

where A_m represents the amplitude, $\mathbf{w}_m^H \mathbf{a}_m(\psi)$ is the transmission gain obtained by the transmitted phased array, d_{T_m} represents the position of the array element of the m-th transmitted channel, t_{delay} represents the time delay of the signal, and ω_d is the normalized Doppler frequency caused by the relative motion between the target and the platform.

To differentiate the echo data of different waveforms, the received signal needs to be filtered using the matched filter $h_m(t) = Q_m(t)\exp(j2\pi f_m t)$; after matched filtering and down-conversion, the array-pulse level echo signal of a target or clutter receiving patch can be expressed as:

$$\begin{aligned} r_m(r,\psi) &= A_m \mathbf{w}_m^H \mathbf{a}_m(\psi) \exp\left(-j\tfrac{2\pi}{\lambda} d_{T_m} \cos\psi\right) \exp(-j4\pi(m-1)\Delta f r/c) \\ &\quad \times \exp(-j\pi\cos\psi(n-1)) \exp(-j\pi\omega_d(k-1)) \\ &= (A_m b_m(\psi) \cdot c_m(\psi) \cdot z_m(r)) \exp(-j\pi\cos\psi(n-1)) \exp(-j\pi\omega_d(k-1)) \\ &= A_m s_{Tr_m}(\psi, r) \exp(-j\pi\cos\psi(n-1)) \exp(-j\pi\omega_d(k-1)) \end{aligned} \tag{12}$$

where $b_m(\psi)$,$c_m(\psi)$ and $z_m(r)$ are assumed as (13) to (15), respectively.

$$b_m(\psi) = \mathbf{w}_m^H \mathbf{a}_m(\psi) \tag{13}$$

$$c_m(\psi) = \exp\left(-j\frac{2\pi}{\lambda} d_{T_m} \cos\psi\right) \tag{14}$$

$$z_m(r) = \exp(-j4\pi(m-1)\Delta f r/c) \tag{15}$$

$\mathbf{b}(\psi)$, $\mathbf{c}(\psi)$, and $\mathbf{z}(r)$ are defined as the transmission coherence accumulation vector, the transmission waveform diversity vector, and the transmission spatial steering vector, respectively, as shown in the following equations:

$$\mathbf{b}(\psi) = \begin{bmatrix} \mathbf{w}_1^H \mathbf{a}_1(\psi) & \mathbf{w}_2^H \mathbf{a}_2(\psi) & \cdots & \mathbf{w}_M^H \mathbf{a}_M(\psi) \end{bmatrix}^T \tag{16}$$

$$\mathbf{c}(\psi) = \begin{bmatrix} \exp\left(-j\tfrac{2\pi}{\lambda} d_{T_1} \cos\psi\right) & \cdots & \cdots & \exp\left(-j\tfrac{2\pi}{\lambda} d_{T_M} \cos\psi\right) \end{bmatrix}^T \tag{17}$$

$$\mathbf{z}(r) = \begin{bmatrix} 1 & \exp(-j4\pi\Delta f r/c) & \cdots & \exp(-j4\pi(M-1)\Delta f r/c) \end{bmatrix}^T \tag{18}$$

According to (16) to (18), $\mathbf{s}_{Tr}(\psi, r)$ could be defined as the transmitting spatial steering vector, and it can be found that the steering vector has two independent variables, which are slant distance r and cone angle ψ, respectively.

$$\mathbf{s}_{Tr}(\psi, r) = \mathbf{b}(\psi) \odot \mathbf{c}(\psi) \odot \mathbf{z}(r) \tag{19}$$

The array level data of the m-th received waveform is expressed in vector form and can be expressed as:

$$\mathbf{r}_m(t,\psi) = A_m s_{Tr_m}(\psi, R_r) \cdot \mathbf{s}_{\mathrm{Re}}(\psi) \tag{20}$$

The data received by the antenna array elements are synthesized according to the form of subarray division, and the synthesis matrix $\mathbf{T}$ used for data synthesis can be expressed as:

$$\mathbf{T} = \begin{bmatrix} \mathbf{T}_1 & \mathbf{T}_2 & \cdots & \mathbf{T}_M \end{bmatrix} \tag{21}$$

Each column of the synthetic matrix represents the weighting of one of the subarray data in the following way:

$$\mathbf{a}_m(\psi) = \left[0_{1\times m} \quad 1 \quad e^{-j\pi\cos\psi} \quad \cdots \quad e^{-j\pi(M_n-1)\cos\psi} \quad 0_{1\times(N-M_n+1)}\right]^T \tag{22}$$

$$\mathbf{w}_m = \left[0_{1\times m} \quad w_1 \quad w_2 \quad \cdots \quad w_{M_n-1} \quad 0_{1\times(N-M_n+1)}\right]^T \tag{23}$$

$$\mathbf{T}_m = \mathbf{w}_m \odot \mathbf{a}_m(\psi) \tag{24}$$

where $\mathbf{a}_m(\psi)$ is the local spatial steering vector of each array element in the m-th subarray, $\mathbf{w}_m$ denotes the weight coefficient considered for the synthesis of the m-th subarray, and Chebyshev weights are used uniformly in this paper. The vector form of the subarray level data after pre-processing of the signal of the m-th waveform can be expressed as:

$$\mathbf{r}_{m\_sub}(r,\psi) = A_m \mathbf{s}_{Tr_m}(\psi, r) \cdot \mathbf{T}^H \mathbf{s}_s(\psi) \tag{25}$$

Based on the above steps to match filtering, down-conversion, and data subarray synthesis for M transmitted waveforms, respectively, the virtual data can be expressed in the form of vectors as follows:

$$\mathbf{r}_{sub}(r,\psi,\omega_d) = \mathbf{s}_t(\omega_d) \otimes \left((\mathbf{A}\mathbf{s}_{Tr}(\psi, r)) \otimes \mathbf{T}^H \mathbf{s}_{\mathrm{Re}}(\psi)\right) \tag{26}$$

Due to the radar received data being a superposition of several clutter receiving patches, moving targets, interference and noise, the received data can be expressed as:

$$\mathbf{r}_{sub} = \sum_{j=1}^{N_r}\sum_{i=1}^{N_c} \mathbf{r}_{sub}\left(r,\psi_i,\omega_{d_i}\right) + \sum_{j=1}^{N_{tar}} \mathbf{r}_{sub}\left(r,\psi_j,\omega_{d_j}\right) + \mathbf{n} = \mathbf{x}_c + \mathbf{x}_t + \mathbf{n} \tag{27}$$

3. Different Multi-Domain Signal Processing Methods Based on FDA-Phase-MIMO Radar

Unlike the conventional phased array radar with 2D data in the received array domain-received pulse domain, the FDA-Phase-MIMO radar introduces the transmitting carrier frequency domain to use the coupling relationship between the stepping frequency and the slant distance of received cell, and the data are pre-processed and converted into 3D data in the transmitting carrier frequency domain-received element domain-pulse domain. Figure 3 represents the basic structure of the FDA-Phase-MIMO radar multi-domain processing, where each dimension can be represented as two domains by a set of Fourier transform relations. In this paper, the symbol "-" and symbol "&" are used for cascade processing and joint processing, respectively. In this section, the classical multi-domain clutter suppression methods that have been proposed to be commonly used for non-side-looking AEWRs in the past are briefly described. Then, different 3D joint dimensionality reduction adaptive processing methods are analyzed, and a joint dimensionality reduction structure with performance and lower number of auxiliary channels is proposed.

Method 1: In the past, the first proposed method was the 3D conventional filtering method, i.e., transmitted carrier frequency-received element-received pulse domain 3D conventional filtering method (Figure 3: (1.a)-(2.a)-(3.a)).

A 3D conventional steering vector is constructed, where the received subarray equivalent phase-centered spatial steering vector can be expressed as:

$$\mathbf{s}_{sub} = \left[e^{-j\frac{2\pi}{\lambda}p_1\cos\psi} \quad e^{-j\frac{2\pi}{\lambda}p_2\cos\psi} \quad \cdots \quad e^{-j\frac{2\pi}{\lambda}p_M\cos\psi}\right]^T \tag{28}$$

where $\mathbf{p}_{sub} = \left[p_1 \quad p_2 \quad \cdots \quad p_m\right]^T$ is the equivalent phase center position of each subarray. Then, the 3D conventional filter can be expressed as follows:

$$\mathbf{w}_{pdf}(r,\psi,\omega_d) = \mathbf{s}_t(\omega_d) \otimes (\mathbf{s}_{Tr}(\psi, r) \otimes \mathbf{s}_{sub}(\psi)) \tag{29}$$

The output power spectrum of method 1 can be expressed as:

$$y(r, \psi, \omega_d) = \mathbf{w}_{pdf}^H(r, \psi, \omega_d)\mathbf{r}_{sub} \tag{30}$$

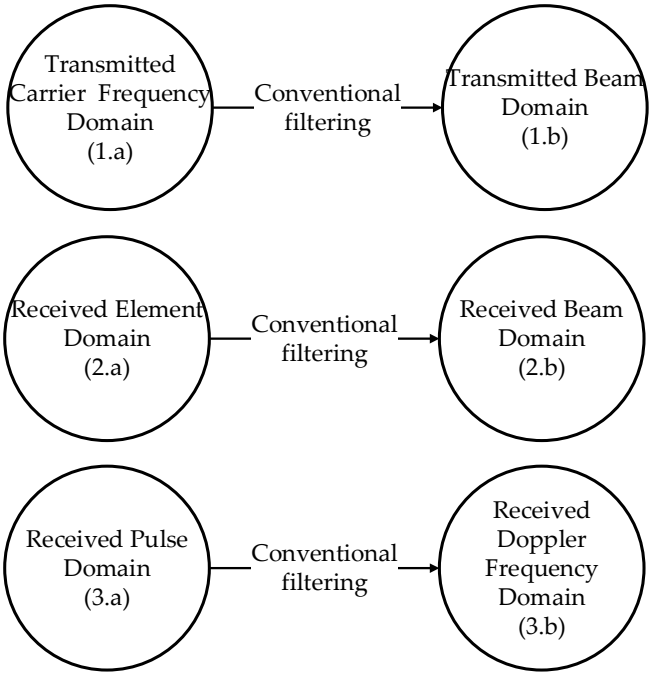

Figure 3. Multi-domain signal processing architecture.

Method 2: In recent years, the conventional processing cascade 2D adaptive processing for clutter suppression method has also been proposed, i.e., transmitted carrier frequency domain 1D conventional filtering and received beam-received Doppler frequency domain 2D downscaling adaptive processing (Figure 3: (1.a)-(2.b) & (3.b)).

After pre-processing means, such as matched filtering and down-conversion, the $M^2K \times 1$ dimensional virtual data of the CUT cell can be expressed as:

$$\mathbf{r}_{sub} = \mathbf{x}_c + \mathbf{x}_t + \mathbf{n} \tag{31}$$

The 3D virtual data by selecting a fixed transmitted carrier frequency domain filter can be expressed as:

$$\mathbf{w}_{Tr}(\psi, r) = diag(1_{K\times 1} \otimes (\mathbf{s}_{Tr}(\psi, r) \otimes 1_{M\times 1})) \tag{32}$$

The processed data can be expressed as follows:

$$\mathbf{y}(\psi, r) = \mathbf{w}_T^H(\psi, r)\mathbf{r}_{sub} \tag{33}$$

Next, according to $\hat{y}_i(\psi, r) = y_{Mi}(\psi, r)$, $i = 1, 2, \cdots, MK$, the data $\mathbf{y}(\psi, r)$ of dimension $M^2K \times 1$ is rewritten as $\hat{\mathbf{y}}(\psi, r)$. The space–time 2D adaptive weight and the output power spectrum of the system are calculated and can be expressed, respectively, as:

$$\mathbf{w}_{st}(\psi, \omega_d) = \beta \mathbf{R}_{cn}^{-1}\mathbf{s}_{st}(\psi, \omega_d) \tag{34}$$

$$z(r, \psi, \omega_d) = \mathbf{w}_{st}^H(\psi, \omega_d)\hat{\mathbf{y}}(\psi, r) \tag{35}$$

where $\mathbf{s}_{st}(\psi, \omega_d)$ is the 2D steering vector for the target.

Method 3: Transmitted beam-received beam domain-received Doppler frequency domain 3D joint downscaling adaptive processing (Figure 3: (1.b) & (2.b) & (3.b)) is proposed.

Instead of forming a conventional beam in the newly introduced transmitted carrier frequency dimension, this method takes advantage of the adaptive processing approach and uses the additional DOFs coming from the stepped carrier frequency to form an adaptive beam. According to Figure 3, it can be seen that 3D adaptive processing of the data can be performed in 8 combinatorial domains by means of permutations. Due to the fact that full adaptive processing is often not feasible in reality [23,28–31], to reduce the DOFs of the received clutter and the number of I.I.D. samples required for CCM estimation, the received clutter data is dimensionality reduced in all three dimensions, and the data is converted to the transmitted beam-received beam domain-received Doppler frequency domain for signal processing, i.e., The transformation matrix for each domain is constructed based on the principle of the selection of auxiliary channels. The result of dimensionality reduction of the transmitted carrier frequency steering vector using the dimensionality reduction matrix is:

$$\tilde{\mathbf{u}} = \mathbf{T}_T^H \mathbf{u}(\psi, r) \tag{36}$$

The result of dimensionality reduction of the received element steering vector can be expressed as:

$$\tilde{\mathbf{s}}_s = \mathbf{T}_R^H \mathbf{s}_s \tag{37}$$

Finally, the received pulse domain is downscaled and converted to the received Doppler frequency domain:

$$\tilde{\mathbf{s}}_t = \mathbf{T}_t^H \mathbf{s}_t \tag{38}$$

According to (36) to (38), the dimensionality reduction matrix in three dimensions is (39), and (40) represents the conversion relationship between the domain (1.a)-(2.a)-(3.a) and domain (1.b)-(2.b)-(3.b):

$$\tilde{\mathbf{s}}_t \otimes \left(\tilde{\mathbf{u}} \otimes \tilde{\mathbf{s}}_s\right) = \left(\mathbf{T}_t^H \mathbf{s}_t\right) \otimes \left(\left(\mathbf{T}_T^H \mathbf{u}\right) \otimes \left(\mathbf{T}_R^H \mathbf{s}_s\right)\right) = \mathbf{T}^H(\mathbf{s}_t \otimes (\mathbf{u} \otimes \mathbf{s}_s)) \tag{39}$$

The 3D dimensionality reduction transformation matrix can be expressed as:

$$\mathbf{T} = (\mathbf{T}_t \otimes (\mathbf{T}_T \otimes \mathbf{T}_R)) \tag{40}$$

Based on the two commonly used dimensionality reduction structures in the 2D-STAP method, it is first simply extended to the 3D-JDL method and 3D-generalized adjacent multi-beam (3D-GMB) method in this paper.

Method 3.a: 3D-JDL method: The principle of selecting auxiliary channels for the 3D-JDL method is shown in Figure 4a,c–e, where the target unit and its neighboring units are selected as auxiliary channels. This section sets the total number of auxiliary channels to $Q_{Tr} \times Q_{\mathrm{Re}} \times Q_t$ (in Figure 4, the number of auxiliary channels is 3∗3∗3). The 3D steering vector of the target can be expressed as $\mathbf{u}(\psi_t, r_t)$, $\mathbf{s}_s(\psi_t)$, and $\mathbf{s}_t\left(\omega_{d_t}\right)$, respectively. In order to select the appropriate auxiliary channel, the 3D reduction matrix should be expressed as:

$$\mathbf{T}_T = \left[\mathbf{u}(\psi_t, r_t - \Delta r) \quad \mathbf{u}(\psi_t, r_t) \quad \mathbf{u}(\psi_t, r_t + \Delta r)\right]_{M\times 3} \tag{41}$$

$$\mathbf{T}_R = \left[\mathbf{s}_s(\psi_t - \Delta\psi) \quad \mathbf{s}_s(\psi_t) \quad \mathbf{s}_s(\psi_t + \Delta\psi)\right]_{M\times 3} \tag{42}$$

$$\mathbf{T}_t = \left[\mathbf{s}_t\left(\omega_{d_t} - \Delta\omega_d\right) \quad \mathbf{s}_t\left(\omega_{d_t}\right) \quad \mathbf{s}_t\left(\omega_{d_t} + \Delta\omega_d\right)\right]_{K\times 3} \tag{43}$$

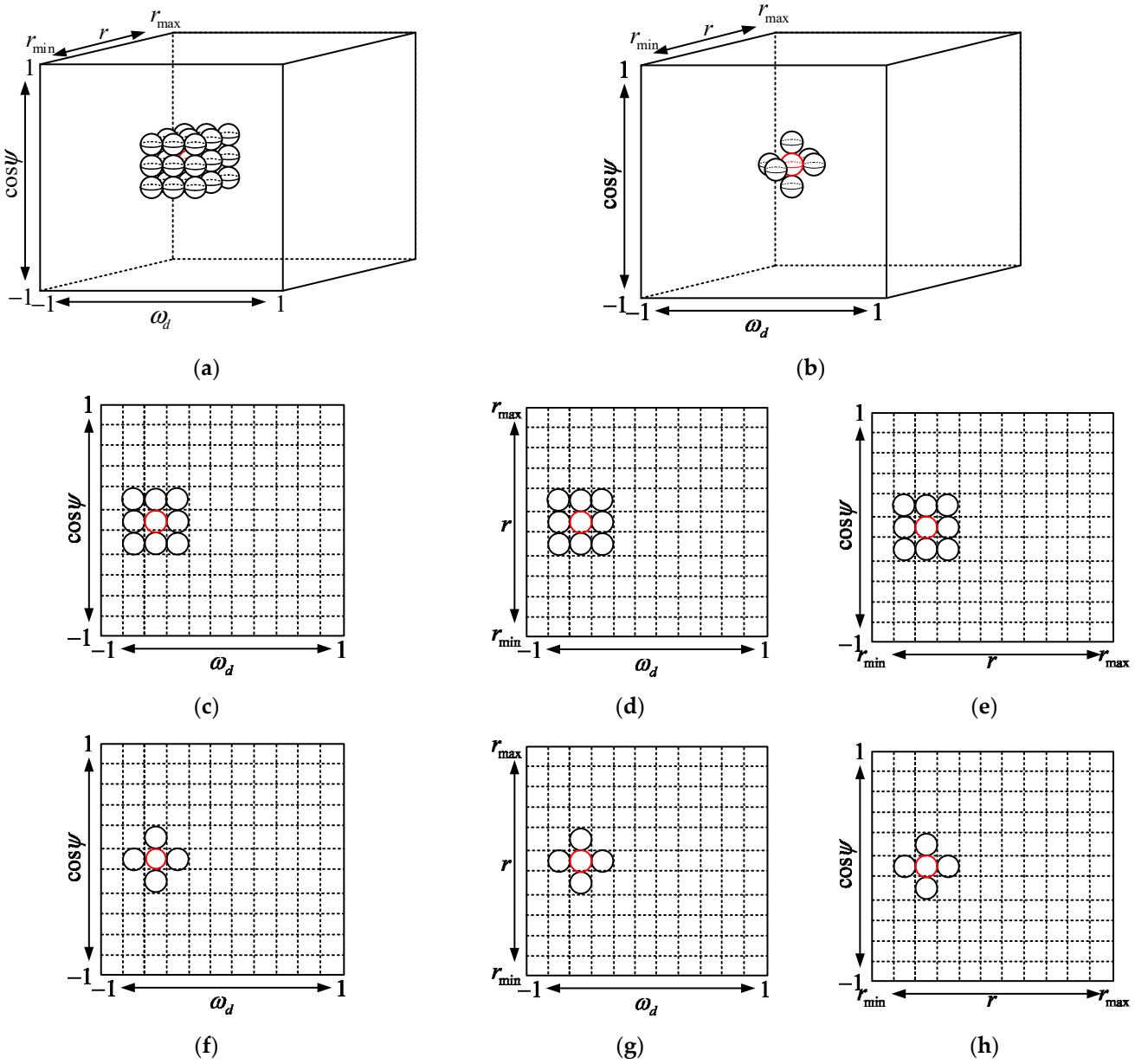

Figure 4. Auxiliary channel selection structure for different dimensionality reduction method: (**a**) Method 3.a; (**b**) Method 3.b; (**c**–**e**) Downscaling structure in different domain of method 3.a; (**f**–**h**) Downscaling structure in different domain of method 3.b.

The 3D dimension reduction matrix of the 3D-JDL method can be expressed as:

$$\mathbf{T}_{3a} = [\mathbf{T}_t \otimes (\mathbf{T}_T \otimes \mathbf{T}_R)]_{M^2K \times 27} \tag{44}$$

And the transformational domain data can be expressed as:

$$\mathbf{x}_{JDL} = {\mathbf{T}_{3a}}^H \mathbf{r}_{sub} \tag{45}$$

with an adequate number of training samples satisfying the I.I.D. condition, the estimated CCM obtained using the maximum likelihood estimation method can be expressed as:

$$\hat{\mathbf{R}}_{cn} = \frac{1}{P} \sum_{p=1}^{P} \mathbf{x}_{JDL_p} \mathbf{x}_{JDL_p}^H \tag{46}$$

Method 3.b: 3D-GMB method: The principle of selecting auxiliary channels for the 3D-GMB method is shown in Figure 4b,f,h. This section sets the total number of auxiliary channels to $Q_{Tr} + Q_{\mathrm{Re}} + Q_t - 2$ (in Figure 4, the number of auxiliary channels is 3 + 3 + 3 − 2). To select the appropriate auxiliary channel, the 3D reduction matrix should be expressed as:

$$\begin{aligned}\mathbf{T}_{3b} = \big[&\mathbf{s}(\psi_t, r_t, \omega_{d_t})\mathbf{s}(\psi_t, r_t, \omega_{d_t} + \Delta\omega_d)\mathbf{s}(\psi_t, r_t, \omega_{d_t} - \Delta\omega_d)\ldots \\ &\mathbf{s}(\psi_t, r_t + \Delta r, \omega_{d_t})\mathbf{s}(\psi_t, r_t - \Delta r, \omega_{d_t})\mathbf{s}(\psi_t + \Delta\psi, r_t, \omega_{d_t})\,\mathbf{s}(\psi_t - \Delta\psi, r_t, \omega_{d_t})\big]_{M^2K\times 7}\end{aligned} \tag{47}$$

The transformational domain data after downscaling can be expressed as:

$$\mathbf{x}_{GMB} = {\mathbf{T}_{3b}}^H \mathbf{r}_{sub} \tag{48}$$

In the same way as (46), the estimated CCM obtained using the maximum likelihood estimation method can be expressed as:

$$\hat{\mathbf{R}}_{cn} = \frac{1}{P}\sum_{p=1}^{P} \mathbf{x}_{GMB_p}\mathbf{x}_{GMB_p}^H \tag{49}$$

In addition, there are two problems in selecting training samples for SBEWR to meet the I.I.D. condition: firstly, the number of samples available in an unambiguous distance is limited, and the SBEWR has more obvious clutter non-uniformity due to its wider coverage region, which is prone to the problem of insufficient training samples leading to the degradation of clutter suppression performance. Secondly, the larger the number of training samples selected, the more the effect of non-stationary characteristics on the accuracy of the estimation of CCM cannot be ignored. Therefore, a criterion for selecting the number of clutter auxiliary channels is proposed in this paper, i.e., under the criterion that the DOFs of the system is substantially larger than the DOFs of the local clutter; the smaller the number of auxiliary channels selected, the easier the method is to implement in practical work. Therefore, the required number of auxiliary channels between the 3D-JDL method and the 3D-GMB method are considered, both of which are proposed in this paper, as shown in Figure 5.

Method 3.c: The selected auxiliary channel dimension reduction structure is shown in Figure 5a,c,e. The 2D-GMB method is applied in the received beam-received Doppler plane where the target is located, and the 2D-JDL method is applied in two other 2D planes. The composition of the dimensionality reduction matrix is as follows:

$$\begin{aligned}\mathbf{T}_1(r_t) = \big[&\mathbf{s}(\psi_t, r_t, \omega_{d_t})\mathbf{s}(\psi_t, r_t, \omega_{d_t} + \Delta\omega_d)\mathbf{s}(\psi_t, r_t, \omega_{d_t} - \Delta\omega_d)\ldots \\ &\mathbf{s}(\psi_t + \Delta\psi, r_t, \omega_{d_t})\,\mathbf{s}(\psi_t - \Delta\psi, r_t, \omega_{d_t})\big]_{M^2K\times 5}\end{aligned} \tag{50}$$

$$\begin{aligned}\mathbf{T}_2(r_t + \Delta r) = \big[&\mathbf{s}(\psi_t, r_t + \Delta r, \omega_{d_t})\mathbf{s}(\psi_t, r_t + \Delta r, \omega_{d_t} + \Delta\omega_d)\ldots \\ &\mathbf{s}(\psi_t, r_t + \Delta r, \omega_{d_t} - \Delta\omega_d)\mathbf{s}(\psi_t + \Delta\psi, r_t + \Delta r, \omega_{d_t})\;\mathbf{s}(\psi_t - \Delta\psi, r_t + \Delta r, \omega_{d_t})\big]_{M^2K\times 5}\end{aligned} \tag{51}$$

$$\begin{aligned}\mathbf{T}_3(r_t - \Delta r) = \big[&\mathbf{s}(\psi_t, r_t - \Delta r, \omega_{d_t})\mathbf{s}(\psi_t, r_t - \Delta r, \omega_{d_t} + \Delta\omega_d)\;\ldots \\ &\mathbf{s}(\psi_t, r_t - \Delta r, \omega_{d_t} - \Delta\omega_d)\mathbf{s}(\psi_t + \Delta\psi, r_t - \Delta r, \omega_{d_t})\,\mathbf{s}(\psi_t - \Delta\psi, r_t - \Delta r, \omega_{d_t})\big]_{M^2K\times 5}\end{aligned} \tag{52}$$

The total dimensionality reduction matrix $\mathbf{T}_{3c}$ can be expressed as:

$$\mathbf{T}_{3c} = [\mathbf{T}_1(r_t - \Delta r)\;\mathbf{T}_2(r_t)\;\mathbf{T}_3(r_t + \Delta r)] \tag{53}$$

The transformational data can be expressed as:

$$\hat{\mathbf{x}}_{3c} = {\mathbf{T}_{3c}}^H \mathbf{r}_{sub} \tag{54}$$

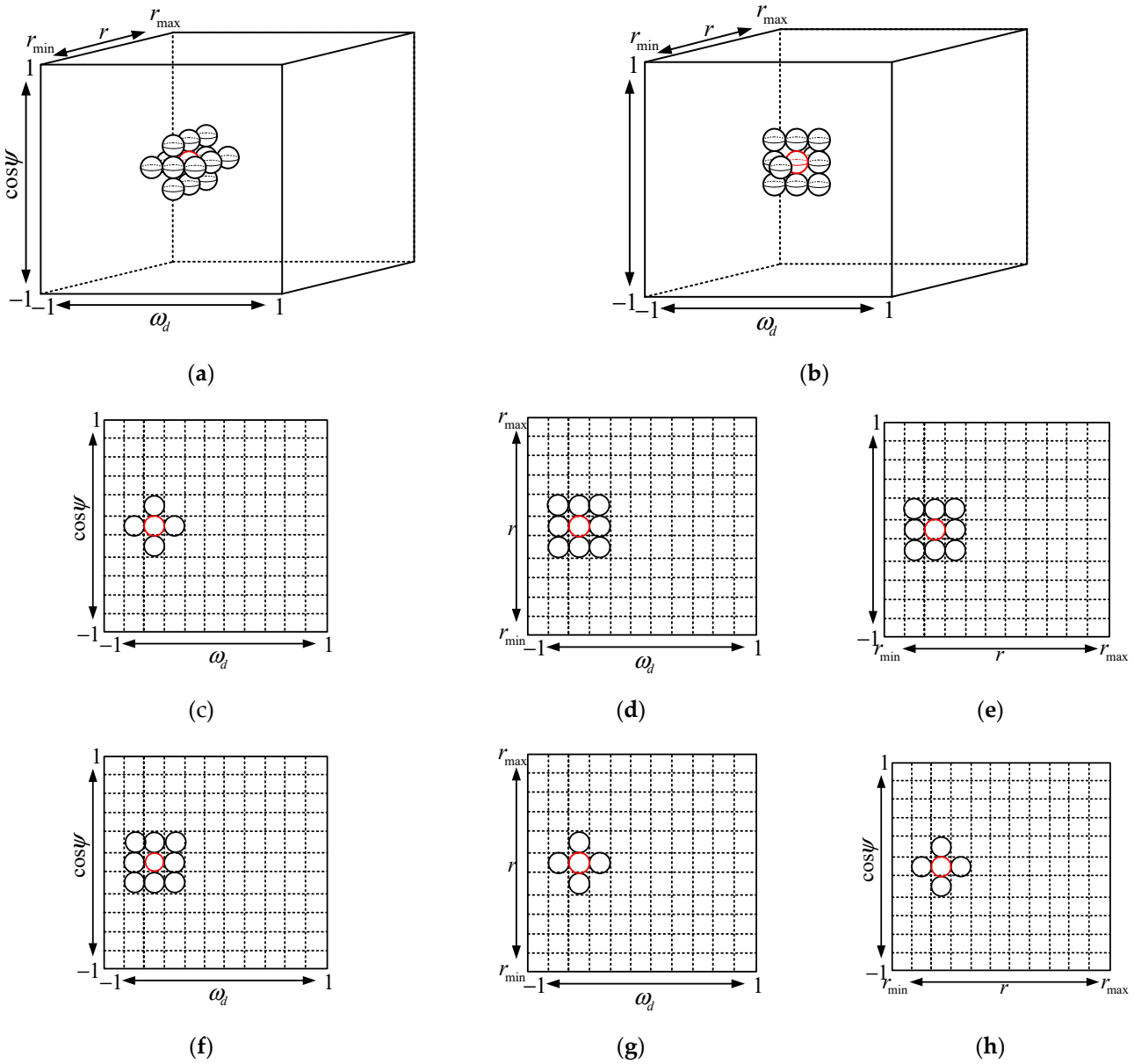

Figure 5. Auxiliary channel selection structure for different dimensionality reduction method: (**a**) Method 3.c; (**b**) Method 3.d; (**c**–**e**) Downscaling structure in different domain of method 3.c; (**f**–**h**) Downscaling structure in different domain of method 3.d.

Method 3.d: The selected auxiliary channel dimension reduction structure is shown in Figure 5a,f,h. The 2D-JDL method is applied in the received beam-received Doppler plane where the target is located, and the 2D-GMB method is applied in two other 2D planes. The composition of the downscaling matrix is as follows:

$$\mathbf{T}_T = [\mathbf{u}(\psi_t, r_t)]_{M\times 1} \tag{55}$$

$$\mathbf{T}_R = \begin{bmatrix}\mathbf{s}_s(\psi_t - \Delta\psi) & \mathbf{s}_s(\psi_t) & \mathbf{s}_s(\psi_t + \Delta\psi)\end{bmatrix}_{M\times 3} \tag{56}$$

$$\mathbf{T}_t = \begin{bmatrix}\mathbf{s}_t(\omega_{d_t} - \Delta\omega_d) & \mathbf{s}_t(\omega_{d_t}) & \mathbf{s}_t(\omega_{d_t} + \Delta\omega_d)\end{bmatrix}_{K\times 3} \tag{57}$$

The 3D dimensionality reduction matrix of the 3D-JDL method can be expressed as:

$$\mathbf{T} = [\mathbf{T}_t \otimes (\mathbf{T}_T \otimes \mathbf{T}_R)]_{M^2K\times 9} \tag{58}$$

The total dimensionality reduction matrix $\mathbf{T}_{3d}$ can be expressed as:

$$\mathbf{T}_{3d} = \begin{bmatrix} \mathbf{T} & \mathbf{s}\left(\psi_t, r_t + \Delta r, \omega_{d_t}\right) & \mathbf{s}\left(\psi_t, r_t - \Delta r, \omega_{d_t}\right) \end{bmatrix} \tag{59}$$

The transformation data can be expressed as:

$$\hat{\mathbf{x}}_{3d} = {\mathbf{T}_{3d}}^H \mathbf{r}_{sub} \tag{60}$$

4. Simulation Results and Discussion

In this section, some classical methods are simulated and validated, and their advantages and disadvantages are demonstrated as well as their feasibility when suffering the SBEWR clutter environment. According to the publicly available basic parameters provided by the NASA space-based demonstration validation radar and the prior work by authors on SBEWR [32,33], the discussion and signal processing method simulation validation of SBEWR in this paper are based on the parameters provided in Table 1. The non-stationary characteristics of received clutter are considered, while the clutter non-uniformity problem due to the rapid change of clutter terrain is ignored, and this premise will not affect the argument of the reliability of the proposed method in the experiment. The amplitude undulations of received clutter obeyed the Weber distribution, and the moving targets were added to the clutter data according to the parameters in Table 2.

Table 1. Basic parameters of SBEWR used in this paper.

Type	Parameter	Symbol	Index
Orbital Parameters	Orbit height	H	500 km
	Inclination	i	45°
	Platform Velocity	V	7612 m/s
Signal Parameters	Carrier frequency	f_c	0.55 GHz
	Bandwidth	B	0.8 MHz
	Coherent pulse number	K	32
	PRF	f_r	5000 Hz
	Pulse Width	T_p	20μs
Antenna Parameters	Antenna aperture	$D_a \times D_r$	50 m ∗ 3 m
	Antenna Oblique angle	$\theta_{oblique}$	0°
	Beam scanning range	$\Delta\theta_{el}$ $\Delta\theta_{az}$	EL:30~68° AZ:30~150°
	Channel number	$M_a \times M_r$	16 ∗ 1
	Antenna Pitch angle	φ	90°
	Beam direction	θ_{el_0} θ_{az_0}	EL: 46° AZ: 90°

Table 2. Parameters of the moving target in the simulation experiment.

No.	Range Bin Number	Slant Distance (km)	Radial Velocity (m/s)	Normalized Doppler Frequency	RCS (m^2)
1	1740	761	1026	−0.5	10
2	1820	773	2590	−0.2	0.1
3	1870	780.5	−1602	−0.35	1

The theoretical distribution of clutter receiving patches and moving targets in the range-Doppler (R-D) output power spectrum is shown in Figure 6a. Moreover, this distribution is related to the basic parameters such as SBEWR platform parameters and pulse parameters, and not related to whether a conventional phased array radar or an FDA-Phase-MIMO radar is used. In the absence of clutter, the simulated moving target in the R-D output power spectrum is shown in Figure 6b.

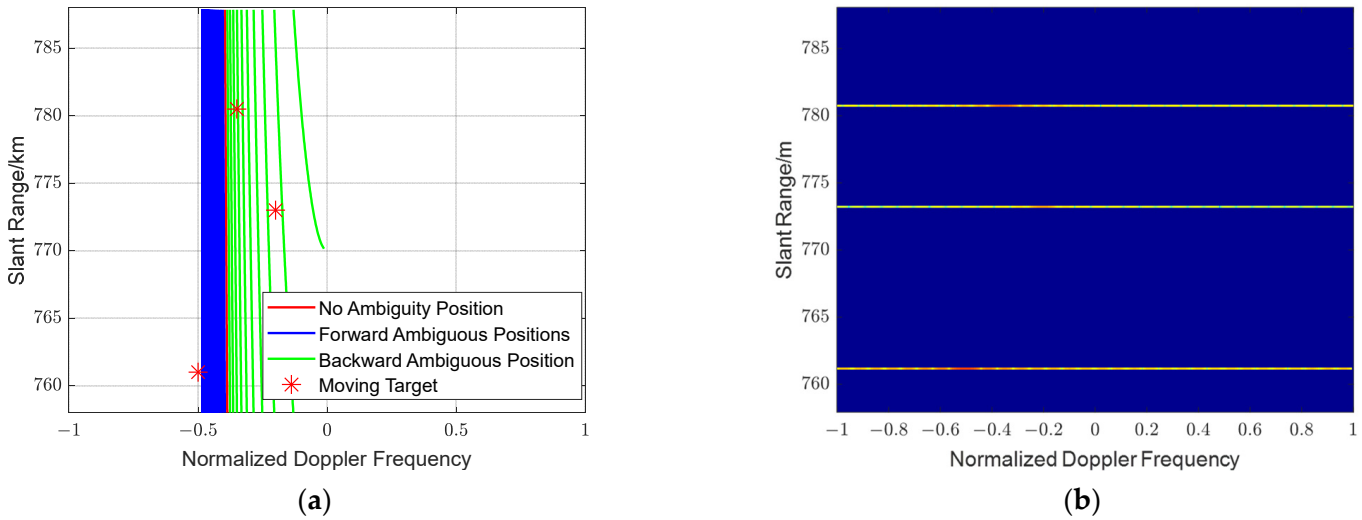

Figure 6. Range-Doppler output power spectrum: (**a**)Theoretical spectrum of received clutter and moving target; (**b**) Simulation spectrum with moving target.

In Figure 6a, the red line represents the Doppler distribution of clutter receiving patches at different range cells within an unambiguous distance corresponding to the center of the beam, and each of the other lines represent the Doppler distribution of clutter receiving patches in different range ambiguous intervals. The forward range ambiguous positions are discrete, and many backward range ambiguous positions of the clutter receiving patches in the Doppler dimension cannot be distinguished; the distribution of the clutter Doppler dimension at different range ambiguous positions is consistent with the distribution of the ambiguous positions in the elevation angle dimension expressed in (5). From the distribution position information of clutter and moving targets in Figure 6a, it can be found that the faint moving target energy is often submerged in the clutter due to the very large amount of range ambiguous position energy of SBEWR spreading severely in the Doppler dimension.

In this paper, only the non-stationary and range ambiguity characteristics of clutter are considered, and in this uniform clutter scenario, the clutter received energy is inversely proportional to the fourth power of the slant distance. Moreover, according to the relationship between the beam grazing angle and the clutter backscattering coefficient in the clutter Morchin model, it is known that the inverse relationship between the energy of the clutter unit at the forward ambiguous position and the clutter energy of the CUT is greater than the fourth power of the distance. Moreover, the elevation dimensional gain direction provided by different regime radars are different, and the clutter received cell with a slant distance of 771 km is used as the CUT, and the ratio of different range ambiguous positions and CUT clutter energy is shown in Figure 7.

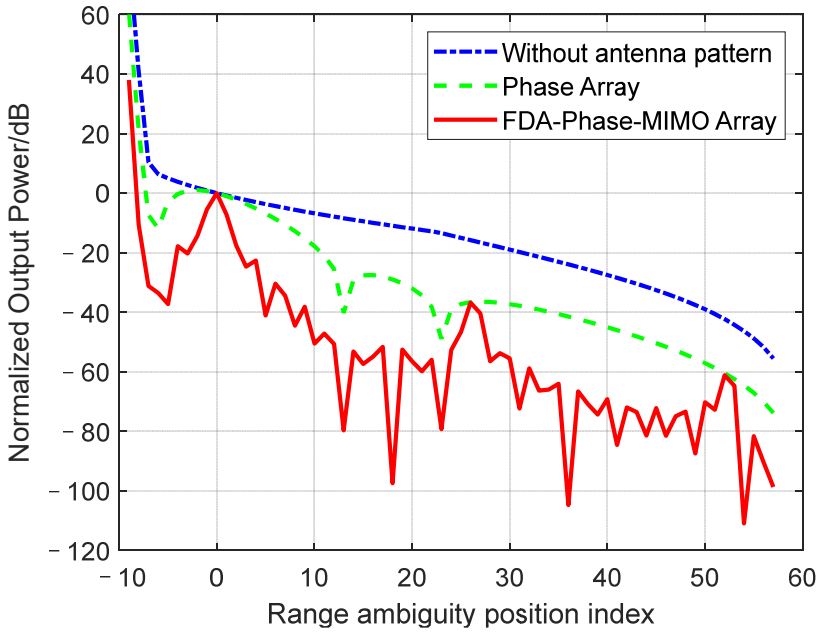

Figure 7. Normalized clutter power of clutter receiving units at different range ambiguous positions.

In Figure 7, the power between each range ambiguous position and CUT is shown in the blue line. It can be found that the clutter energy of the backward ambiguous position is much higher than the energy from the CUT. For the phased-array radars with planar arrays, due to the modulation of the regular beam gain in the elevation dimension, the power is shown in the green line, and for the planar array of FDA-Phase-MIMO radar, by the joint modulation of the elevation dimensional and transmitting carrier frequency directional gain direction, the ambiguous position power is shown in the red line.

In the past, FDA-Phase-MIMO radar uses a conventional beamforming method in the new introduced domain, which can obtain better performance of range ambiguous clutter compared with phased-array radar, but the energy of the clutter from the forward ambiguous position is still high and is in the same order of magnitude as the CUT energy. This phenomenon allows the DOF of received clutter after preprocessing to still be high, i.e., the received CCM is often still nonsingular. Therefore, the method 1 and method 2, using cascaded signal processing illustrated in Section 3, will not obtain good clutter suppression performance.

Figure 8 shows the R-D output power spectrum using 1D conventional filtering-2D adaptive processing (method 2, Figure 3 (1.a)-(2.b) & (3.b)). In Figure 8a, it can be found that part of the moving target information originally covered by ambiguous position clutter energy can be found. However, according to Figure 8b, the target detection performance that can be obtained is insufficient; it is still difficult to reach the threshold required for C-FAR detection with certain detection probability and false alarm probability. Figure 9 represents the eigenvalue spectrum of the CCM, and all the eigenvalue numbers are much higher than the order of magnitude where the noise energy is located, i.e., the CCM is nonsingular, which will lead to the degradation of the adaptive performance.

Through the 3D dimensionality reduction joint adaptive processing method (method 3, Figure 3((1.b)–(3.b)), the radar system could achieve great clutter suppression performance when the auxiliary channel has been selected reasonably. In this section, the performance obtainable by all dimensionality reduction methods is analyzed and compared.

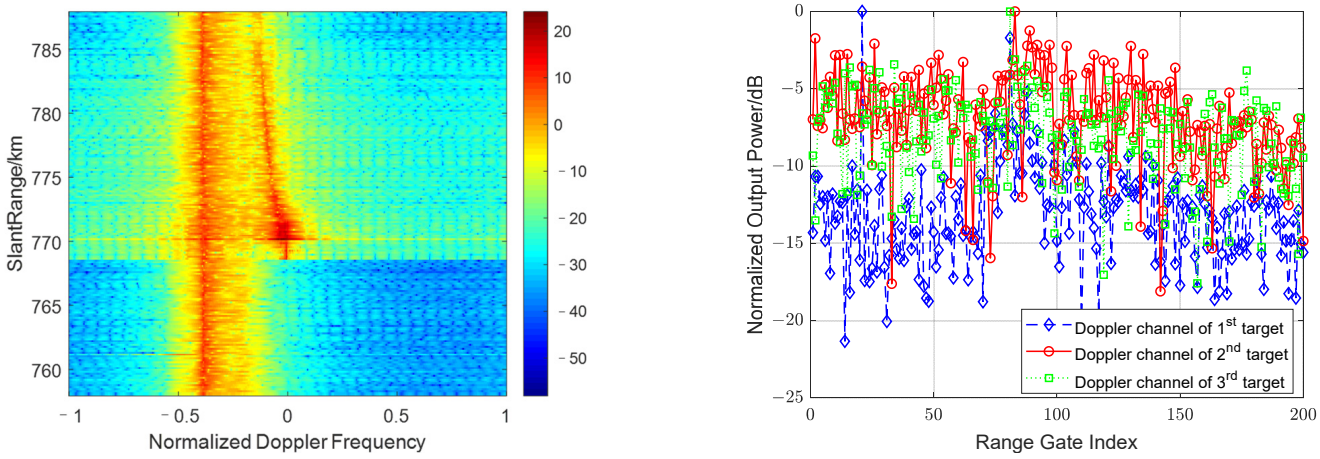

Figure 8. Output power spectrum for FDA-Phase-MIMO SBEWR after method 2: (**a**) Range-Doppler output power spectrum; (**b**) Normalized output power spectrum in different Doppler channels.

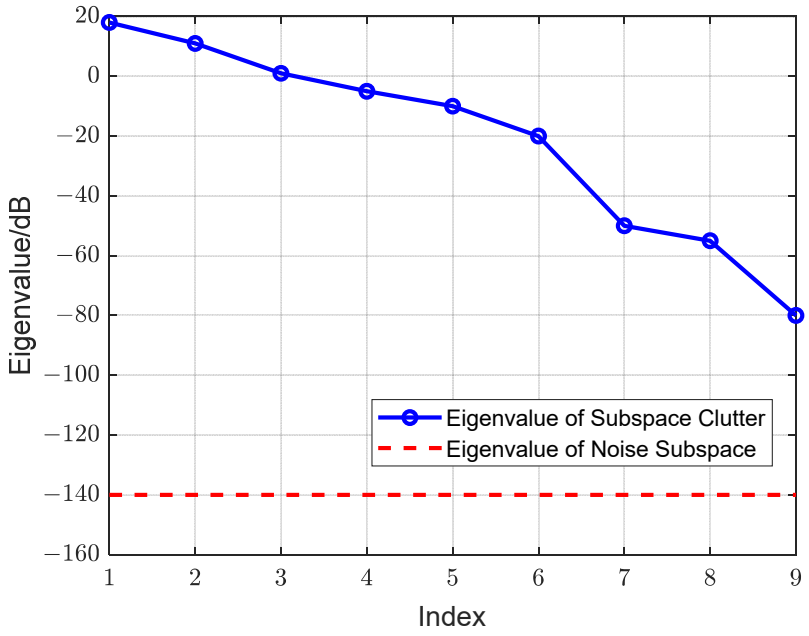

Figure 9. The eigenvalue spectrum of reduced dimensional clutter covariance matrix.

Figures 10a and 11a show the R-D output power spectrum obtained by method 3.a and method 3.b, respectively, and Figures 10b and 11b show the eigenvalue spectrum of the CCM when the target unit is approaching the main clutter. Compared with the past cascaded method, 3D joint adaptive processing has better range ambiguous clutter suppression performance. From the eigenvalue spectrum of the two CCM, it can be found that by using method 3.a, the CCM has more small eigenvalues, i.e., extra available DOFs for adaptive processing, compared to method 3b, which obtains a covariance matrix that does not satisfy the criterion that the DOFs of the system are greater than the DOFs of the clutter.

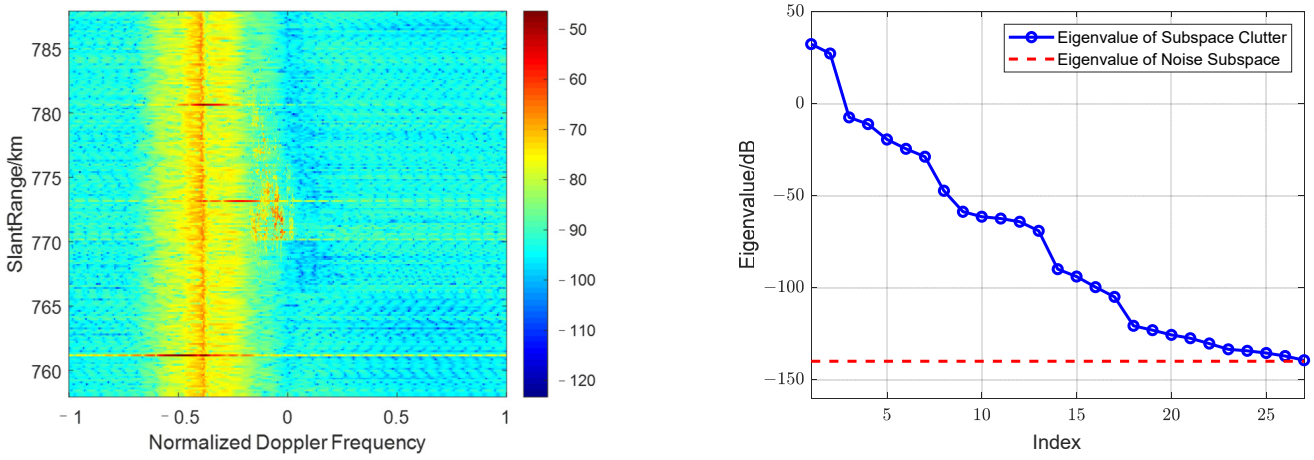

(**a**) (**b**)

Figure 10. (**a**) The range-Doppler output power spectrum after using method 3.a; (**b**) The eigenvalue spectrum of the dimensionality reduction CCM.

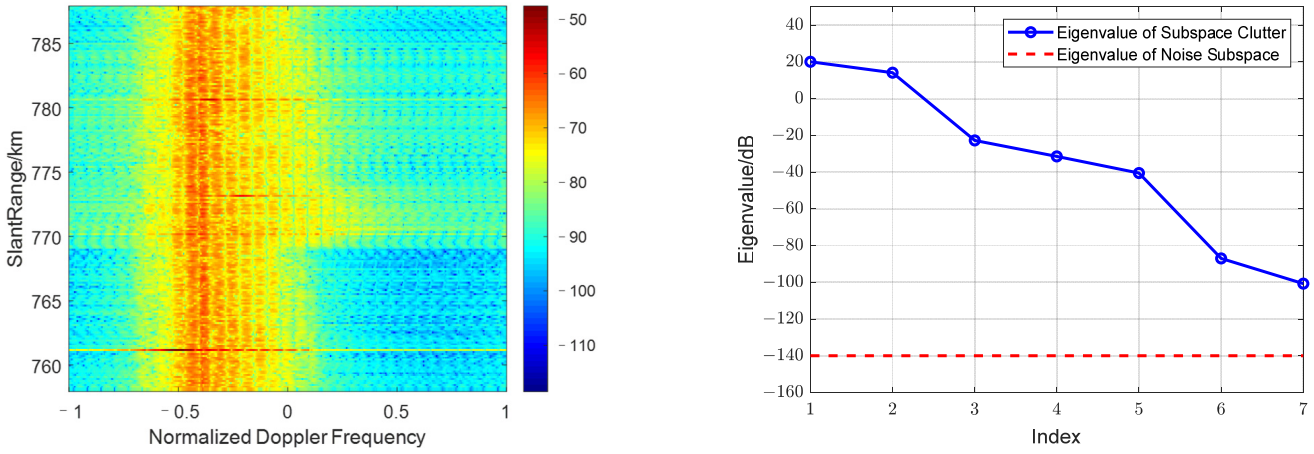

(**a**) (**b**)

Figure 11. (**a**) The range-Doppler output power spectrum after using method 3.b; (**b**) The eigenvalue spectrum of the dimensionality reduction CCM.

Figure 12 shows the normalized output power spectrum obtained by different methods in different Doppler channels where the moving targets are located, respectively. It can be found that using the 3D joint adaptive method can obtain better performance than the cascade method from this figure, and that the performance improvement brought by method 3.a is more obvious.

Next, the performance of two other joint dimensionality reduction methods with the number of auxiliary channels between method 3.a and method 3.b is analyzed. Figures 13a and 14a show the R-D output power spectrum obtained by method 3.c and method 3.d, respectively, and Figures 13b and 14b show the eigenvalue spectrum of the CCM when the dimensionality reduction structure is approaching the main lobe clutter, respectively. From the experimental results, it can be found that method 3.c satisfies the criterion that the DOFs of the system are larger than the DOFs of the clutter, can achieve great clutter suppression performance, and the DOFs of the system are reduced from 27 to 15. With the further reduction of the selected number of auxiliary channels, the DOFs of the system are insufficient, and the clutter suppression performance is decreased by using method 3.d.

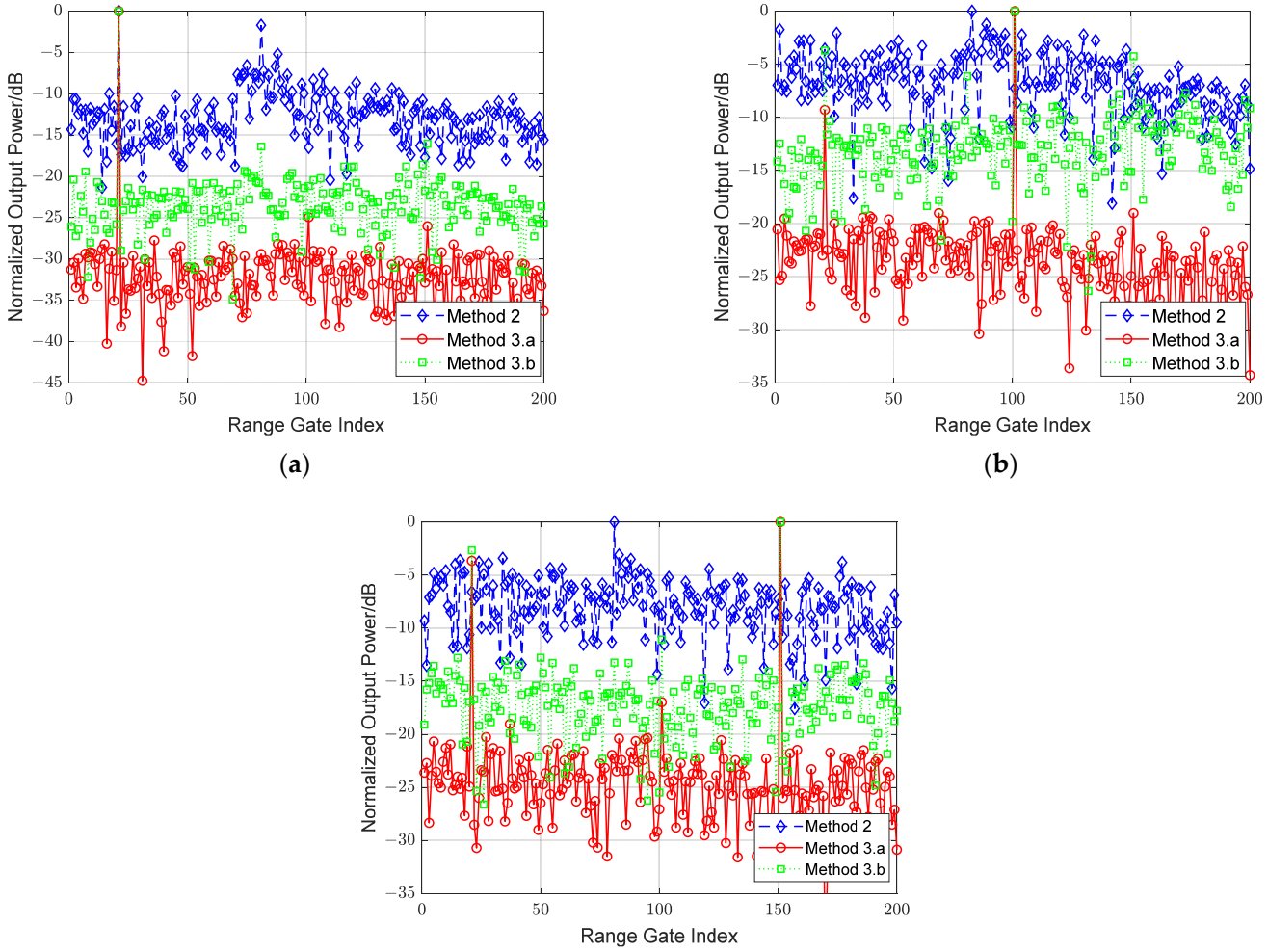

Figure 12. Normalized output power spectrum in different Doppler channels by method 2, 3.a and 3.b: (**a**) Doppler channel of 1st target; (**b**) Doppler channel of 2nd target; (**c**) Doppler channel of 3rd target.

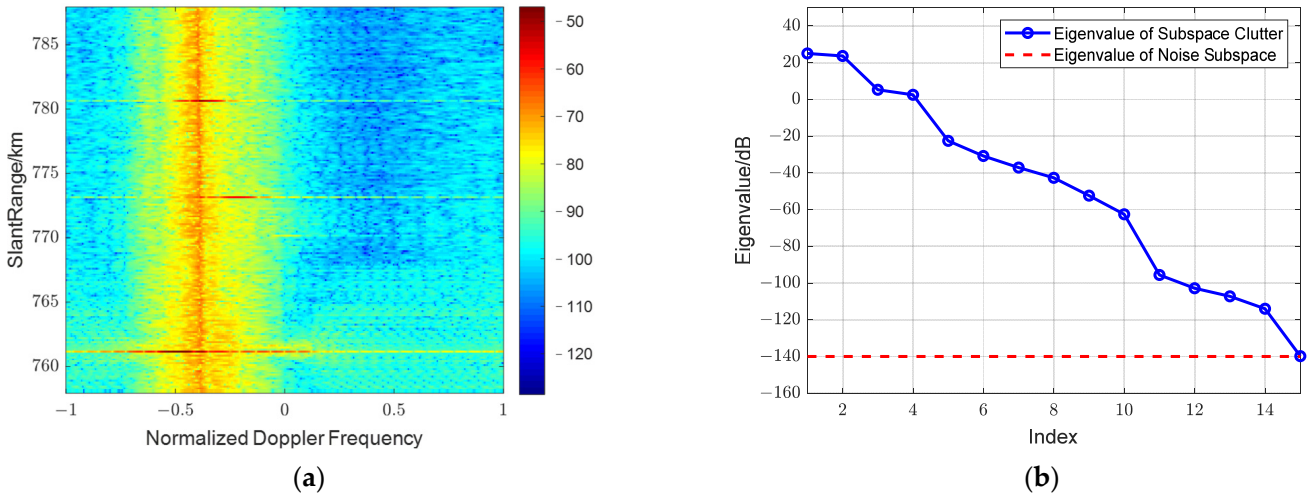

Figure 13. (**a**) The range-Doppler output power spectrum after using method 3.c; (**b**) The eigenvalue spectrum of reduced dimensional clutter covariance matrix.

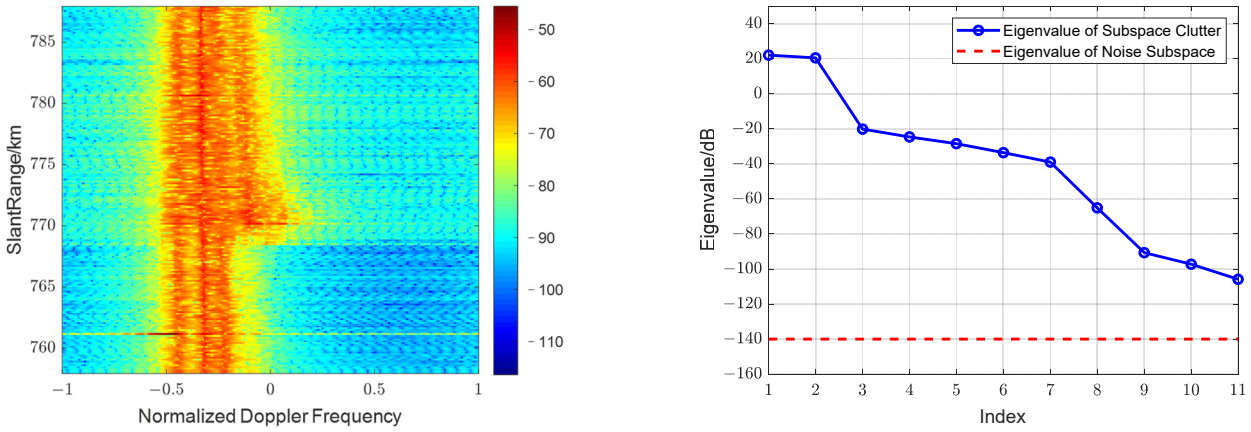

(**a**) (**b**)

Figure 14. (**a**) The range-Doppler output power spectrum after using method 3.d; (**b**) The eigenvalue spectrum of reduced dimensional clutter covariance matrix.

Figure 15 shows the normalized output power spectrum obtained by using different methods in different Doppler channels where the moving targets are located, respectively. The results can be found that the detection of three different moving targets can be achieved by using the reduced structure proposed by method 3.c; while the number of auxiliary channels decreases, the clutter suppression performance of method 3.d decreases, and the moving targets are covered by clutter energy and cannot be detected.

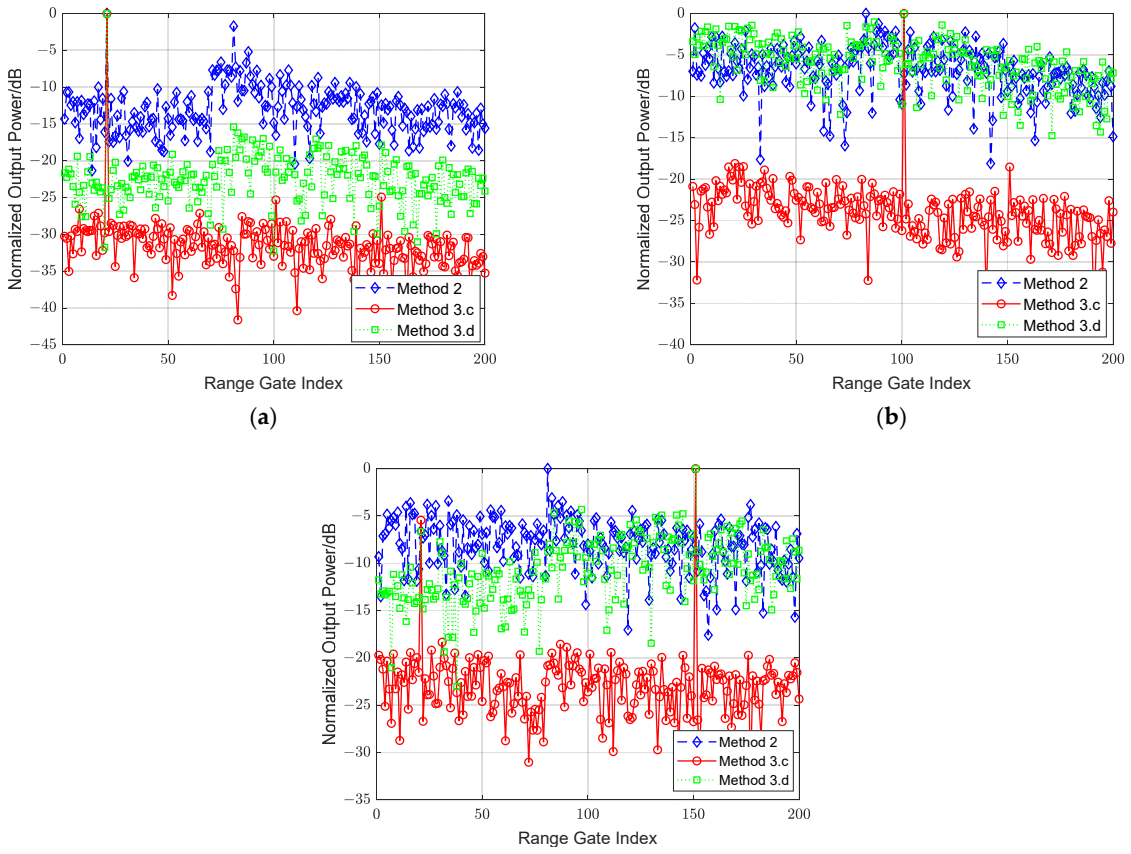

(**a**) (**b**)

(**c**)

Figure 15. Normalized output power spectrum in different Doppler channels by different method 2, 3.c and 3.d: (**a**) Doppler channel of 1st target; (**b**) Doppler channel of 2nd target; (**c**) Doppler channel of 3rd target.

Figure 16 shows the comparison of the moving target detection performance of the two better dimensionality reduction structures. Compared with method 3.a, method 3.c is able to ensure no degradation of the moving target detection performance while significantly reducing the DOFs of the system. In summary, in this paper, method 3.c is considered to be a great multi-domain joint dimensionality reduction structure with comprehensive performance, and the dimensionality structure can achieve better clutter suppression and moving target detection performance.

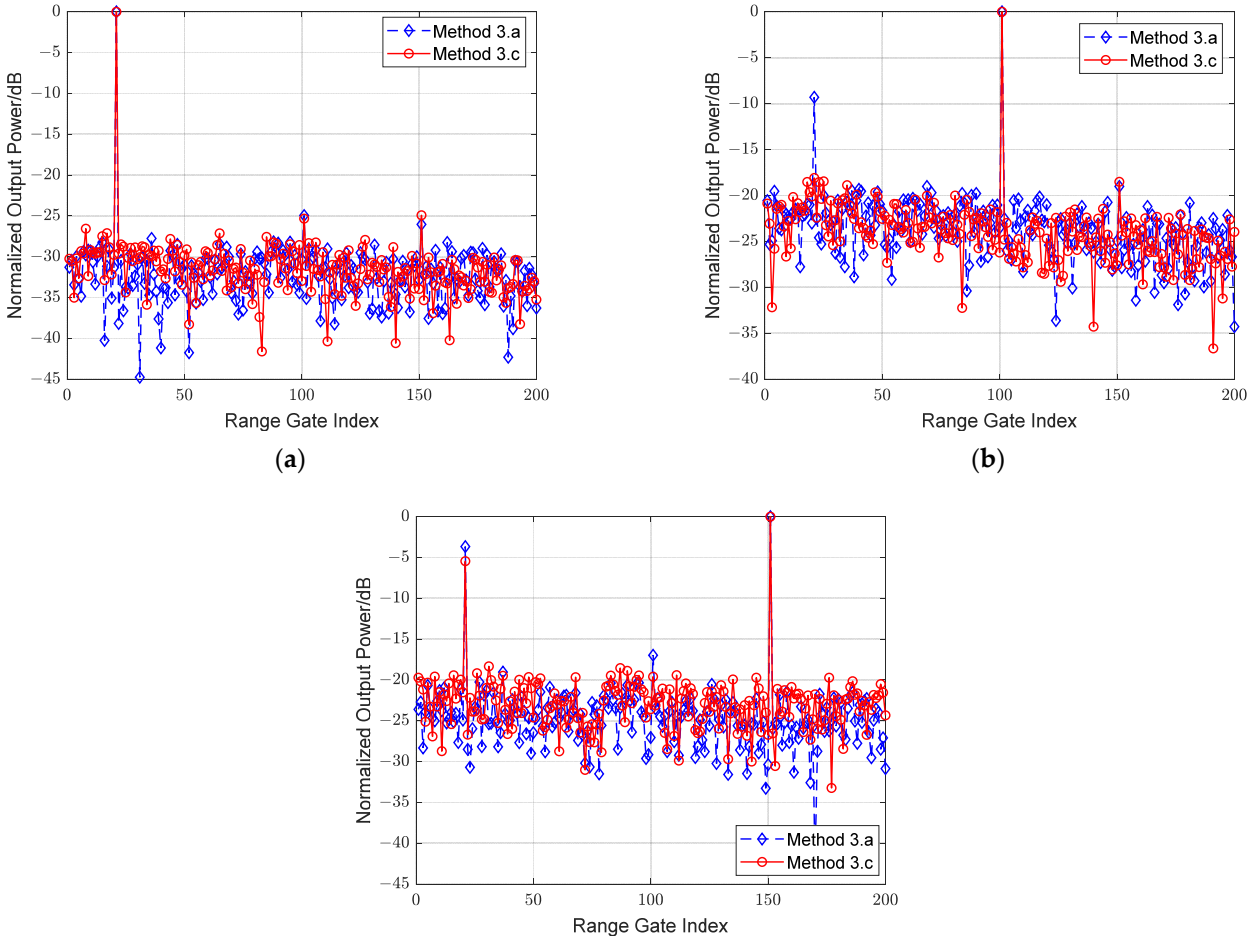

Figure 16. Normalized output power spectrum in different Doppler channels by method 3.a and 3.c: (**a**) Doppler channel of 1st target; (**b**) Doppler channel of 2nd target; (**c**) Doppler channel of 3rd target.

Finally, to further illustrate the advantages of the proposed method, the clutter suppression and moving target detection capabilities that could be obtained in the past by introducing the 3D-JDL-STAP method in the elevation-dimensional channel domain are used for comparison. The elevation-dimensional size of the antenna set up for this experiment is 3 m, and the number of its elevation-dimensional channels is eight. Figure 17a shows the R-D output power spectrum obtained by the traditional elevation-dimensional 3D-JDL-STAP method.

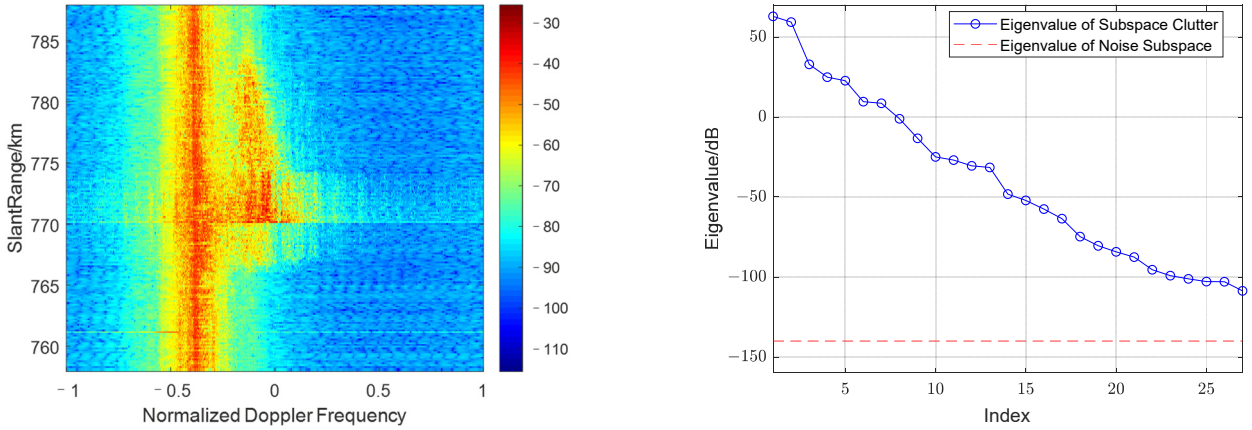

(**a**) (**b**)

Figure 17. (**a**) The range-Doppler output power spectrum after using traditional elevation 3D-JDL-STAP; (**b**) The eigenvalue spectrum of reduced dimensional clutter covariance matrix.

It can be found through Figure 17b that since the covariance matrix of the subspace clutter is nonsingular, which represents the lack of additional DOFs for the adaptive system to accurately suppress the received clutter, the clutter in the near-end range ambiguous positions is difficult to be suppressed and the overall clutter suppression performance is reduced significantly. Figure 18 shows the output power spectrum of the Doppler channels where different moving targets are located, respectively, and it can be seen that the faint moving targets in the near-end range ambiguous positions and near the main lobe region are difficult to be detected using the traditional 3D joint adaptive processing method.

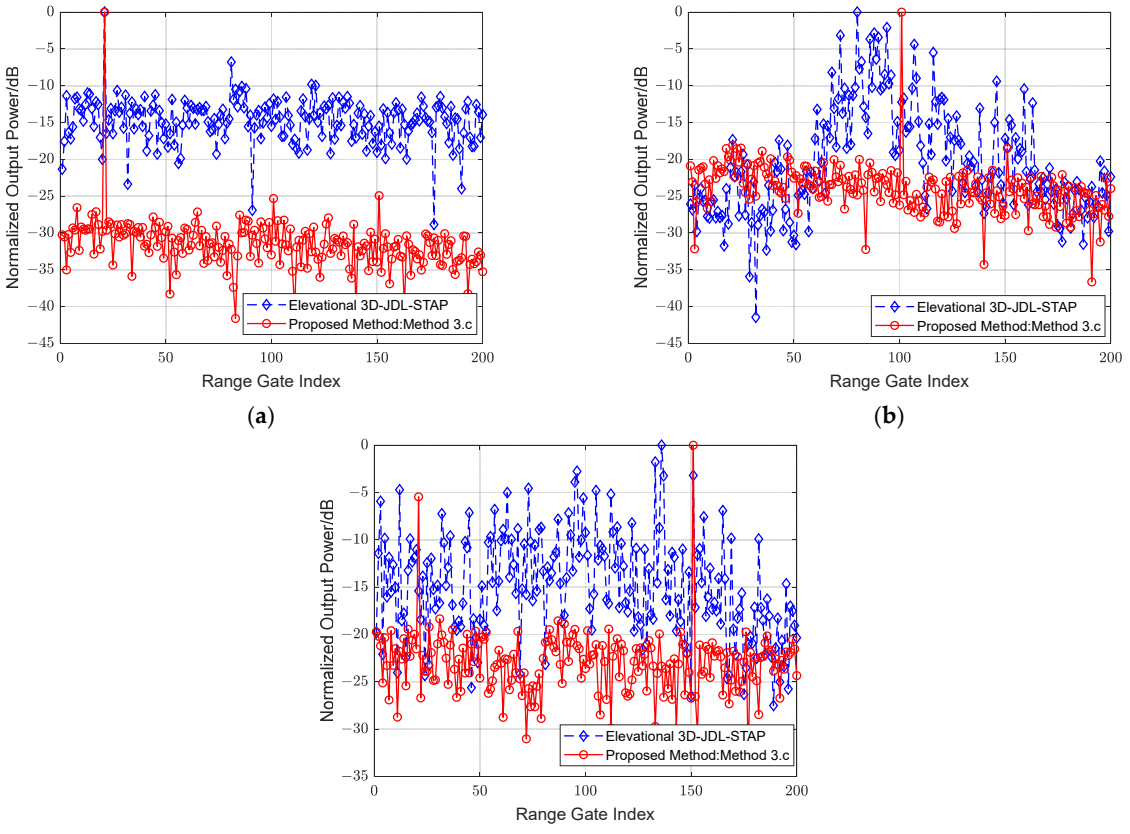

(**a**) (**b**)

(**c**)

Figure 18. Normalized output power spectrum in different Doppler channels by different method: (**a**) Doppler channel of 1st target; (**b**) Doppler channel of 2nd target; (**c**) Doppler channel of 3rd target.

In summary, the performance of moving target detection obtained by the proposed method and former clutter suppression methods for non-side-looking AEWRs are compared. After the clutter is suppressed by different methods, the detection performance obtained by the conventional C-FAR method is shown in Table 3, where the P_d and P_{fa} represent the probability of detection and false alarm, respectively.

Table 3. The performance of faint moving target detection by different methods.

Method		Target 1	Target 2	Target 3
FDA: Cascaded processing (method 2)	Threshold	11 dB	/	/
	P_d	50%	/	/
	P_{fa}	10^{-4}	/	/
Elevation: 3D-JDL-STAP	Threshold	11 dB	/	/
	P_d	50%	/	/
	P_{fa}	10^{-4}	/	/
Proposed Method (method 3.c)	Threshold	25 dB	20 dB	20 dB
	P_d	$> 95\%$	$> 85\%$	$> 85\%$
	P_{fa}	10^{-6}	10^{-6}	10^{-6}

5. Conclusions

In this paper, the main problem faced by SBEWR clutter suppression is clarified, and to achieve better performance of clutter suppression and moving target detection, a new processing dimension must be introduced for severely range ambiguous clutter suppression. The following conclusions can be found in the experimental results in Section 4:

(a) The non-stationary factors lead to serious range ambiguous clutter spreading, the DOFs of received clutter are greatly expanded, and the clutter suppression performance of both conventional phased array radar and FDA-Phase-MIMO radar using cascade processing method is limited by the DOFs of the radar system.
(b) For SBEWRs, especially for higher orbits, as the number of range ambiguous positions increases, a greater number of transmitting carrier frequencies are needed to increase the DOFs of the adaptive system. The performance of the method of obtaining adaptive processing dimensions using the limited elevation-dimensional channels will be further degraded.
(c) The 3D joint dimensionality reduction method needs to satisfy the criterion that the DOFs of the system are larger than the DOFs of the local clutter when selecting the auxiliary channels. Otherwise, it will cause performance degradation.
(d) With sufficient DOFs of the signal processing system, the smaller number of auxiliary channels chosen for the dimensionality reduction method, the smaller number of training samples it requires, and the less significant the error in the estimation of the CCM caused by non-stationary factors.

In addition, for the joint adaptive processing method, a reduced-dimensional structure with 15 degrees of freedom of the proposed system can achieve good clutter suppression and moving target detection performance, and according to the R.M.B. criterion, the number of training samples required for estimating training samples is less, and the proposed method is more suitable for space-based early warning radar.

Author Contributions: The contribution of authors is stated as follows: methodology and formulation, T.Z. and Y.W.; software realization, T.Z.; validation and experiments, T.Z.; writing and review, T.Z. and Z.W.; funding acquisition, M.X. and S.Z. All authors have read and agreed to the published version of the manuscript.

Funding: This research is supported by the National Science Fund for Distinguished Young Scholars under Grant 61825105, the National Natural Science Foundation of China under Grant 61801387.

Data Availability Statement: Not applicable.

Conflicts of Interest: The authors declare no conflict of interest.

References

1. Davis, M.E. Space Based Radar Moving Target Detection Challenges, Radar. In Proceedings of the 2002 International Radar Conference, Edinburgh, UK, 15–17 October 2002; pp. 143–147. [CrossRef]
2. Chamberlain, N.; Amaro, L.; Oakes, E.; Hodges, R.; Spitz, S.; Rosen, P.A. Microstrip patch antenna panel for large aperture L-band phased array. In Proceedings of the IEEE Aerospace Conference, Big Sky, MT, USA, 5–12 March 2005; pp. 1185–1192.
3. Podvig, P. The operational status of the Russian space-based early warning system. *Sci. Glob. Secur.* **1994**, *4*, 363–384. [CrossRef]
4. Zhang, H.; Liu, W.; Shi, J.; Fei, T.; Zong, B. Joint Detection Threshold Optimization and Illumination Time Allocation Strategy for Cognitive Tracking in a Networked Radar System. *IEEE Trans. Signal Process.* **2022**, 1–15. [CrossRef]
5. Li, H.; Liao, G.; Xu, J.; Lan, L. An Efficient Maritime Target Joint Detection and Imaging Method with Airborne ISAR System. *Remote Sens.* **2022**, *14*, 193. [CrossRef]
6. Han, J.; Cao, Y.; Wu, W.; Wang, Y.; Yeo, T.-S.; Liu, S.; Wang, F. Robust GMTI Scheme for Highly Squinted Hypersonic Vehicle-Borne Multichannel SAR in Dive Mode. *Remote Sens.* **2021**, *13*, 4431. [CrossRef]
7. Huang, P.; Zou, Z.; Xia, X.-G.; Liu, X.; Liao, G.; Xin, Z. Multichannel Sea Clutter Modeling for Spaceborne Early Warning Radar and Clutter Suppression Performance Analysis. *IEEE Trans. Geosci. Remote Sens.* **2011**, *59*, 8349–8366. [CrossRef]
8. Xie, W.; Duan, K.; Wang, Y. Space time adaptive processing technique for airborne radar: An overview of its development and prospects. *J. Radars.* **2017**, *6*, 575–586.
9. Bird, J.S.; Bridgewater, A.W. Performance of space-based radar in the presence of earth clutter. *IEE Proc. F Commun. Radar Signal Process.* **2008**, *5*, 491–500. [CrossRef]
10. Pillai, S.; Himed, B.; Li, K.Y. Effect of earth's rotation and range foldover on space-based radar performance. *IEEE Trans. Aerosp. Electron. Syst.* **2006**, *42*, 917–932. [CrossRef]
11. Hovanessian, S.A.; Jocic, L.B.; Lopez, J.M. Spaceborne radar design equations and concepts. In Proceedings of the 1997 IEEE Aerospace Conference, Dayton, OH, USA, 14–17 July 1997; Volume 1, pp. 125–136.
12. Zulch, P.; Davis, M.; Adzima, L.; Hancock, R.; Theis, S. The Earth rotation effect on a LEO L-band GMTI SBR and mitigation strategies. In Proceedings of the 2004 IEEE Radar Conference, Philadelphia, PA, USA, 26–29 April 2004; pp. 27–32.
13. Tang, C.; Wang, X.; Chen, Z.; Sun, F. Space-Time Clutter Simulation and Characteristics Analysis for SBR. In Proceedings of the 2009 International Joint Conference on Computational Sciences and Optimization, Hainan, China, 24–26 April 2009; pp. 856–858.
14. Wang, Z.; Chen, W.; Zhang, T.; Xing, M.; Wang, Y. Improved Dimension-Reduced Structures of 3D-STAP on Nonstationary Clutter Suppression for Space-Based Early Warning Radar. *Remote Sens.* **2022**, *14*, 4011. [CrossRef]
15. Guerci, J. *Space-Time Adaptive Processing for Radar*, 2nd ed.; Artech House: London, UK, 2014; pp. 115–170.
16. Melvin, W. A stap over view. *IEEE Trans. Aerosp. Elect. Syst.* **2004**, *19*, 19–35. [CrossRef]
17. Klemm, R. *Principles of Space-Time Adaptive Processing*, 3rd ed.; IET: London, UK, 2006; pp. 159–177.
18. Wang, W.; Wan, P.; Zhang, J.; Liu, Z.; Xu, J. Enhanced Pre-STAP Beamforming for Range Ambiguous Clutter Separation with Vertical FDA Radar. *Remote Sens.* **2021**, *13*, 5145. [CrossRef]
19. Chen, W.; Xie, W.; Wang, Y. Short-Range Clutter Suppression for Airborne Radar Using Sparse Recovery and Orthogonal Projection. *IEEE Geosci. Remote Sens. Lett.* **2022**, *19*, 3500605. [CrossRef]
20. Wang, Z.; Xie, W.; Duan, K.; Gao, F.; Wang, Y. Short-range clutter suppression based on subspace projection preprocessing for airborne radar. In Proceedings of the 2016 CIE International Conference on Radar (RADAR), Guangzhou, China, 10–13 October 2016; pp. 1–4.
21. Pillai, S.U.; Himed, B.; Li, K.Y. Orthogonal pulsing schemes for improved target detection in space based radar. In Proceedings of the 2005 IEEE Aerospace Conference, Big Sky, MT, USA, 5–12 March 2005; pp. 2180–2189.
22. Cui, N.; Duan, K.; Xing, K.; Yu, Z. Beam-Space Reduced-Dimension 3D-STAP for Nonside-Looking Airborne Radar. *IEEE Geosci. Remote Sens. Lett.* **2022**, *19*, 3506505. [CrossRef]
23. Duan, K.; Xu, H.; Yuan, H.; Xie, H.; Wang, Y. Reduced-DOF Three-Dimensional STAP via Subarray Synthesis for Nonsidelooking Planar Array Airborne Radar. *IEEE Trans. Aerosp. Electron. Syst.* **2020**, *56*, 3311–3325. [CrossRef]
24. Antonik, P.; Wicks, M.C.; Griffiths, H.D.; Baker, C.J. Range-dependent beamforming using element level waveform diversity. In Proceedings of the International Waveform Diversity Design Conference, Lihue, HI, USA, 1 January 2006; pp. 1–4.
25. Antonik, P.; Wicks, M.C.; Griffiths, H.D.; Baker, C.J. Frequency diverse array radar. In Proceedings of the IEEE Radar Conference, Verona, NY, USA, 24–27 April 2006; pp. 24–27.
26. Xu, J.; Liao, G.; Zhang, Y.; Ji, H.; Huang, L. An Adaptive Range-Angle-Doppler Processing Approach for FDA-MIMO Radar Using Three-Dimensional Localization. *IEEE J. Sel. Top. Signal Process.* **2017**, *11*, 309–320. [CrossRef]
27. Ward, J. Space-time adaptive processing for airborne radar. In Proceedings of the IEE Colloquium on Space-Time Adaptive Processing, London, UK, 6 April 1998.
28. Peckham, C.D.; Haimovich, A.M.; Goldstein, J.S.; Reed, I.S. Reduced-Rank STAP Performance Analysis. *IEEE Trans. Aerosp. Electron. Syst.* **2000**, *36*, 664–676. [CrossRef]

29. Goldstein, J.S.; Reed, I.S.; Scharf, L.L. A multistage representation of the Wiener filter based on orthogonal projections. *IEEE Trans. Inf. Technol.* **1998**, *44*, 2943–2959. [CrossRef]
30. Hale, T.B.; Temple, M.A.; Raquet, J.F.; Oxley, M.E.; Wicks, M.C. Localized three-dimensional adaptive spatial-temporal processing for airborne radar. *IET Radar Sonar Navig.* **2003**, *150*, 18–22. [CrossRef]
31. Hale, T.B.; Temple, M.A.; Wicks, M.C. Clutter suppression using elevation interferometry fused with space-time adaptive processing. *Electron. Lett.* **2001**, *37*, 793–794. [CrossRef]
32. Rosen, P.A.; Davis, M.E. A joint space-borne radar technology demonstration mission for NASA and the Air Force. In Proceedings of the 2003 IEEE Aerospace Conference, Big Sky, MT, USA, 8–13 March 2003; pp. 437–444.
33. Zhang, T.; Wang, Z.; Qiao, N.; Zhang, S.; Xing, M.; Wang, Y. A Novel Clutter Covariance Matrix Estimation Method Based on Feature Subspace for Space-Based Early Warning Radar. *IEEE J. Sel. Top. Appl. Earth Obs. Remote Sens.* **2021**, *14*, 11217–11228. [CrossRef]